J Fluoresc (2017) 27:1855–1869
DOI 10.1007/s10895-017-2123-1

ORIGINAL ARTICLE

Structure-Photoproperties Relationship Investigation of the Singlet Oxygen Formation in Porphyrin-Fullerene Dyads

Emel Önal[1] · Sevinc Zehra Topal[1] · Ismail Fidan[1] · Savaş Berber[2] · Fabienne Dumoulin[1] · Catherine Hirel[1]

Received: 1 February 2017 / Accepted: 24 May 2017 / Published online: 30 June 2017

Abstract A systematic structure-photoproperties relationship study of the interactions of porphyrin-fullerene dyads with molecular oxygen was conducted on a set of three porphyrin-fullerene dyads, as this approach of related applications - oxygen sensitivity and photo-induced singlet oxygen generation - of such dyads remained to be endeavoured. To promote energy transfers between the porphyrin and fullerene units and limit undesired charge separation, a particular attention was devoted to the choice of the solvents for the photoproperties determination. Toluene, in which in addition the compounds investigated are not aggregated, was selected accordingly. The molecular orbital levels and energy gaps of the dyads were determined by electrochemistry and theoretical calculations. Their ground state absorption, steady-state fluorescence-based oxygen sensitivity and photo-induced singlet oxygen generation were determined. The dyads were designed to benefit from a facilitated synthetic porphyrin-fullerene coupling thanks to an easy access to formyl-functionalized porphyrins. The effect of two structural parameters was investigated: the presence of electron-donating hexyloxy chains at the *para* position of the *meso*-phenyl, and the presence of a phenylacetylene spacer. This latest factor appeared to have the most predominant effect on all these properties.

Keywords Porphyrin · Fullerene · Dyad · Singlet oxygen · Fluorescence · Electrochemistry · Oxygen sensor

Introduction

The interactions of molecular oxygen with photosensitisers in their excited states [1] is of crucial importance for several applications such as the photogeneration of singlet oxygen for photodynamic therapy, photocatalysis [2] or the luminescence (fluorescence or phosphorescence)-based oxygen sensing. Porphyrins are chosen as photosensitisers for these applications, and our laboratory is strongly involved in their chemistry for photodynamic therapy [3–5] and oxygen sensing purposes [6, 7].

On the other hand, porphyrin-fullerene dyads or superior arrays are electron donor-acceptor systems, and as such, exhibit properties suitable for light-harvesting purposes, as they can behave as photosynthetic antenna or reaction center mimics [8]. Upon irradiation, fullerene acts as an electron and energy acceptor group from photo-activated donor porphyrin. This can be observed on covalent or supramolecular [9] arrays. The nature of the porphyrin-fullerene linkage (flexible or rigid, linear or not, aromatic, ethylenic or acetylenic) proved to have an important effect on the photophysical properties of such dyads. [10–16] These electron donor-acceptor systems can exhibit synergistic properties higher than the sum of the properties exhibited by each isolated partner [17].

Despite its potential interest asserted by all these considerations, investigation of the interactions of porphyrin-fullerene dyads with molecular oxygen remains unexplored in a systematic manner, a topic we wished to endeavour, with further

Electronic supplementary material The online version of this article (doi:10.1007/s10895-017-2123-1) contains supplementary material, which is available to authorized users.

✉ Sevinc Zehra Topal
sztopal@gtu.edu.tr

✉ Catherine Hirel
chirel@gtu.edu.tr

[1] Department of Chemistry, Gebze Technical University, 41400 Gebze, Kocaeli, Turkey

[2] Department of Physics, Gebze Technical University, 41400 Gebze, Kocaeli, Turkey

photodynamic and optical oxygen sensing usages in mind. A few porphyrin-fullerene dyads have indeed proved to be good singlet oxygen generators [18, 19] occasionally used in photodynamic therapy [20, 21], and were previously used as photoelectrochemical sensors [22] but have never been used-to the best of our knowledge - as optical oxygen sensing purposes. Although it is acknowledged that energy and/or electron transfers in porphyrin-fullerene dyads can be affected and sometimes controlled by *i*) the polarity of the solvent, *ii*) the nature of the porphyrin substituents, *iii*) adjusting the distance between the donor and acceptor, [23] systematic investigations of the effect of structural variations on interactions of photo-excited porphyrin-fullerene dyads with molecular oxygen are less reported and yet still needed. This paper tackles this aspect and reports on detailed fundamental investigations conducted on a set of three dyads (Fig. 1) designed following different considerations:

– The relative synthetic accessibility of dyad **1** vs dyads **2** and **3**. Fullerene reacts with aldehyde functions via the Prato reaction [24, 25], thus aldehyde-functionalized porphyrins are needed. This type of compounds required so far multi-steps syntheses [26–28]. Since we recently developed a straightforward method [29] to introduce aldehyde functions at the *meso*-position of porphyrins, the synthetic limitations became the access to mono-*meso*-brominated porphyrin. As 5-(4-bromophenyl)-10,15,20-triphenylporphyrin (**1-Br**) proved to be tedious to isolate, porphyrin **2-Br**, much easier to purify, was designed. **1-Br** led to dyad **1** while **2-Br** is the precursor of dyads **2** and **3**. The effect of the electron-donating hexyloxy chains (dyads **1** vs **2**) likely to affect the solubility of the dyads and to exert an electron-donating effect on their photoproperties will be accordingly investigated.
– The effect of a phenylacetylene moiety. One of our recent studies demonstrated that the presence of a phenylacetylene moiety at the *meso* position of Pd and Pt porphyrins improved their oxygen sensing efficiency [7], a result in line with other documented results showing that the presence of triple bond on oxygen-sensing cores improves their performances [30]. Hence dyad **3** (Fig. 1) was designed to have the fullerene rigidly bound to the *meso*-position of the porphyrin via a phenylacetylene unit acting as a spacer which increases the electron donor-acceptor distance and the π-π

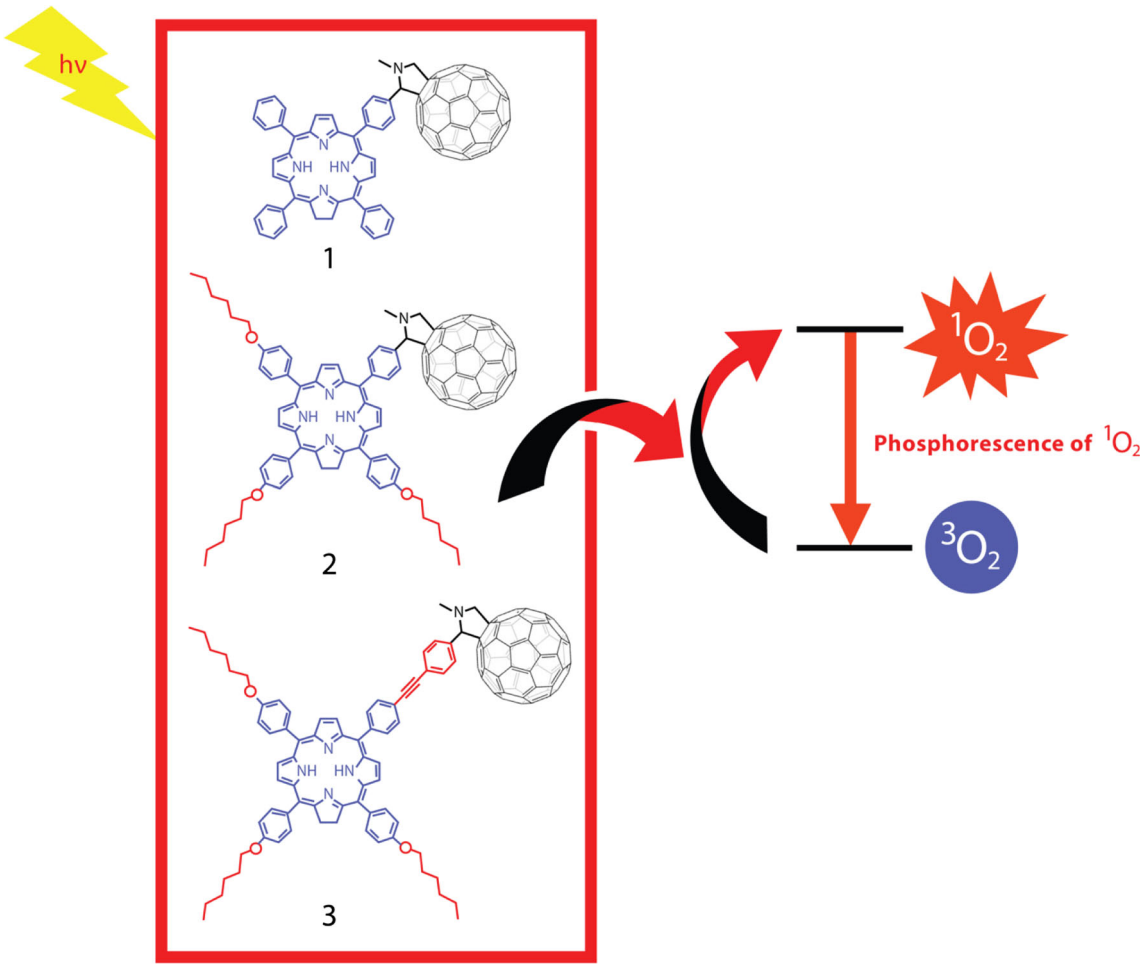

Fig. 1 Targeted fullerene-porphyrin dyads **1**–**3** and their interaction with molecular oxygen

conjugation. The effect of this spacer can be studied by comparing dyads **2** and **3**.

For each dyad, the determination of the photophysical, photochemical and electrochemical behaviour, the molecular orbital levels and energy gaps was comparatively performed with a structure-property relationship approach. A focus of the interactions of the excited states of these three dyads with oxygen was completed with two approaches in mind: their potential use as photodynamic photosensitisers and as molecular oxygen sensors. *Meso*-tetraphenylporphyrin (**TPP**) was used as a reference for all the measurements performed in these works.

Results and Discussion

Synthesis and Chemical Characterization

The synthesis of the novel porphyrin-fullerene dyads (**1–3**) was achieved in two steps, starting from mono-*meso*-brominated porphyrins, **1-Br** or **2-Br** [31]. **1-Br** was prepared by a statistical Adler reaction using a mixture of benzaldehyde and 4-bromobenzaldehyde. As chromatographic separations of **1-Br** from the concomitantly formed *meso*-tetraphenylporphyrin (**TPP**) proved to be really tedious, a clean mixture of **1-Br** and **TPP** was engaged in the next step of the synthesis. **2-Br** was prepared by an alkylation reaction on the trihydroxylated monobrominated derivative **2-Br(OH)3** [5] whose preparation and separation from the symmetrical tetrahydroxylated porphyrin derivative was quite easy thanks to their significantly different polarity. **1-Br** (mixed with TPP) and **2-Br** were subjected to a bromine-lithium exchange reaction previously developed in our group [29], yielding mono-formylporphyrins **1-CHO** or **2-CHO** in 35% and 13% respectively, allowing the introduction of a formyl group directly on the *para* position of the *meso*-phenyl substituent. It has to be noticed that the reactivity of **1-Br** is higher than those of **2-Br**, as shorter reaction time was needed to complete the reaction in higher yield. **2-Br** was also subjected to a Sonogashira reaction with 4-ethynylbenzaldehyde in the presence of $Pd(OAc)_2$, PPh_3, and dry diisopropylamine/THF (1:1 volume), yielding 24% of **3-CHO**, in which the formyl group is away from the porphyrin macrocycle by a phenylacetylide spacer.

The Prato reaction [24, 25], a powerful tool to functionalize fullerene C_{60} sphere by simply refluxing it in the presence of an aldehyde in toluene, led to **1** in 62%, **2** in 45% and **3** in 35% yields (Scheme 1).

All compounds were characterized by IR, ^{1}H NMR and UV-Vis spectroscopies. The IR spectra of formyl-porphyrins **1–3-CHO** show a typical sharp and intense peak at 1694 cm^{-1} which is characteristic of formyl vibration (See supporting information). C_{60} possesses 42 fundamentals of various symmetries, four of them being IR active, at 1428, 1181, 574 and 525 cm^{-1} [32, 33]. Indeed, three IR bands at 1185, 575 and 525 cm^{-1} confirm the successful grafting of the C_{60} on the porphyrins (See supporting information). The success of the coupling was also evidenced by ^{1}H NMR spectroscopy. The well resolved and representative ^{1}H NMR spectra of compound **1-CHO** and dyad **1** are presented in Fig. 2 (See supplementary information for comparative NMR spectra of **2-CHO**, **3-CHO**, dyads **2** and **3**). The integrated peak areas ratio is in agreement with the empirical formula and the AB3 asymmetry. The ^{1}H NMR spectrum of **1-CHO** exhibited six doublets in the aromatic region corresponding to the *meso*-phenyl group protons, two doublets at 7.69 and 8.13 ppm for the 6 protons of the *ortho*-CHAr (H3) and two doublets at 8.21 and 8.32 ppm for *meta*/*para*-CHAr (H4,5). The two doublets at 8.21 and 8.32 ppm are allocated to CHAr (H1 and H2). The eight β pyrrole hydrogen atoms were attributed to two doublets at 8.71 (CH7-pyrrole) and at 8.79 (CH6-pyrrole) as well as a single peak at 8.83 ppm (CH8-pyrrole). Characteristic singlet peak at 10.40 ppm typical of the proton of the formyl groups and the inner NH shielded protons were observed at −2.84 ppm. ^{1}H NMR spectrum of dyad **1** in $CDCl_3/CS_2$ solution is less resolved due to the presence of C_{60} unit, the aromatic signals are broader, but exhibit undoubtedly the expected features and integration ratios. CS_2 is used as a co-solvent to increase the solubility of the dyads. The aromatic protons for the porphyrin moiety were observed at 7.72 ppm (b, 12H, CH4,5-Ar-phenyl), 8.15 ppm (b, 6H, CH3-Ar-phenyl), 8.22 (b, 4H, CH1, 2-Ar-phenyl) and 8.77 (b, 8H, CHpyrrole). Signals of the inner NH were observed at −2.88 ppm. The signals assigned to the pyrrolidine ring can be clearly observed as two doublets at 4.34 and 5.04 (Ha and Hb), a singlet at 5.19 ppm (Hc) and a singlet at 3.09 ppm singlet corresponding to N-CH_3, all in agreement with the literature [34].

Molecular Orbital Levels and Energy Gaps

The band gap energy values define the energy necessary for the transition of an electron from the HOMO to the LUMO. Molecular orbital energy levels and HOMO-LUMO energy gaps give precious information on the potentiality of the dyes for many applications such as solar cells or photosensitiser [35]. The band gap energy was calculated from LUMO and HOMO values obtained by CV as well as theoretical calculations. Calculations of the molecular orbital energy levels and of the energy gaps were performed to quantify the effects of substituent and of the spacer.

Electrochemistry Electrochemistry can be used to characterize and determine the molecular orbital levels and energy gaps of a molecule. C_{60} is one of most popular electron acceptor (A) compound [36] with up to six one-electron reductions whereas free base porphyrins are well-known donors (D) with two oxidations, and particularly with small difference [37] between first and second oxidation when substituents located on the *para* position of

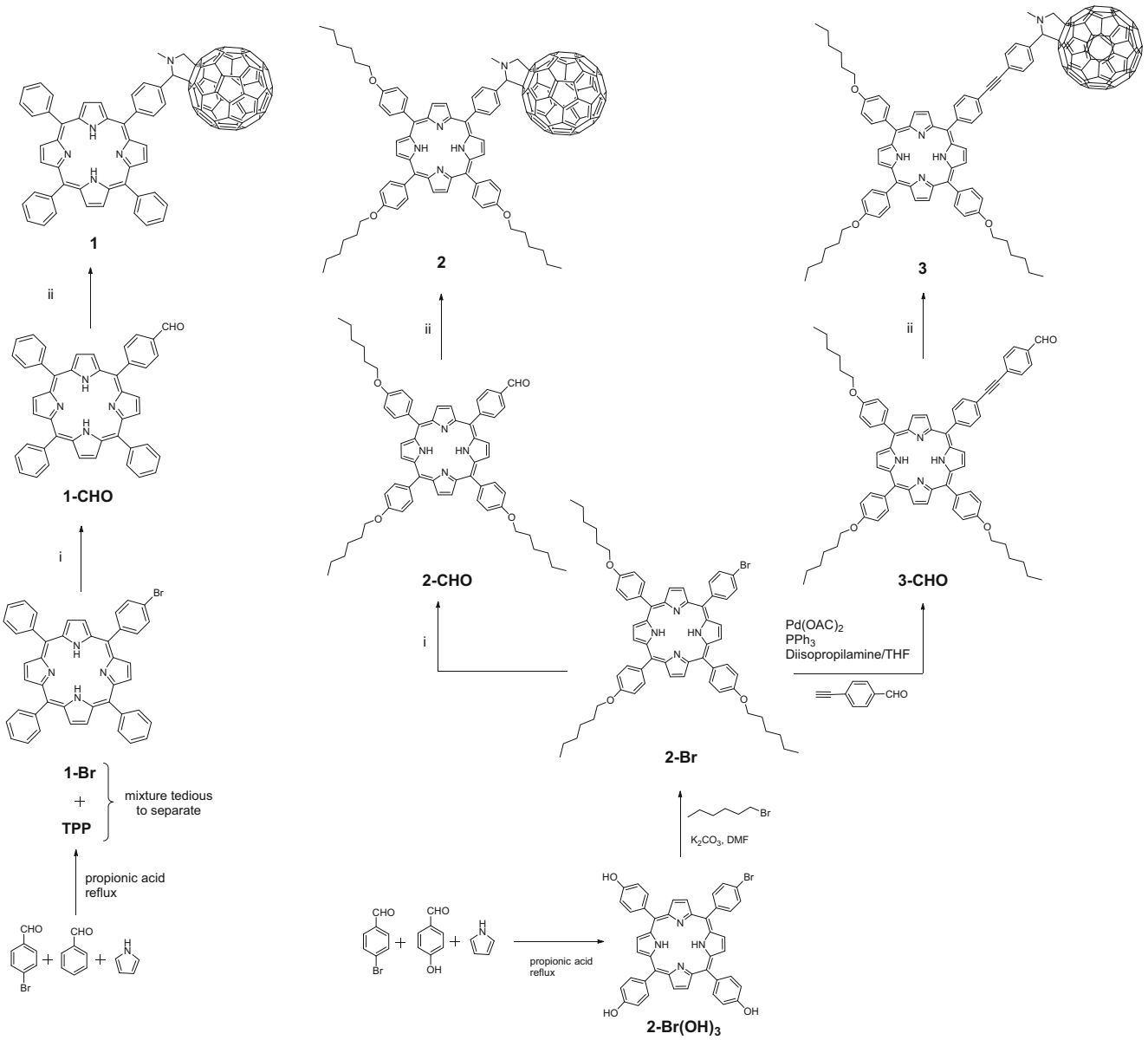

Scheme 1 General synthetic pathway i) *n*-BuLi, Et_2O, DMF, Ar, −50 °C, ii) sarcosine, toluene, reflux

meso-phenyls moieties. The electrochemical behaviour of dyads **1**–**3**, **TPP** and C_{60} were investigated in *o*-dichlorobenzene/acetonitrile (4:1) mixture by using cyclic voltammetry (CV) (Fig. 3).

The oxidation and reduction potentials of dyads **1**–**3** were summarized in Table 1, and match previous literature reports with peaks attributable to the fullerene moieties while the remaining ones are due to the porphyrin [38]. Dyad **1** exhibited four reduction and two oxidation peaks between −2.5 V and +1.0 V. The first oxidation was observed at 0.572 V and, the second one at 0.880 V which were arose from oxidations of porphyrin skeleton. Dyad **2** and **3** showed very similar reduction patterns with small potential shifts. Dyad **2** had lower first oxidation potential (0.416 V) than dyad **1** did (0.572 V), as anticipated, due to the electron-donating nature of the three hexyloxy moieties on *meso*-phenyls of the porphyrin core that caused the 0.156 V shift to negative potentials. First oxidation of dyad **3** occurred at 0.481 V which was higher than that of dyad **2** (0.416 V) but lower than that of dyad **1** (0.572 V) due to the presence of the phenylacetylene spacer which in return avoid lowering the potential. In terms of reductions, the observed first and second reductions of the dyads (for example at −1.134 V and −1.536 V for dyad **1**) correspond to the first and second reduction of fullerene whereas the third one corresponds to the first reduction of the porphyrin macrocycle. However, dyad's fourth reduction was attributed to third reduction of C_{60} and second reduction of porphyrin which were overlapped at −2.076 V. Finally, the electron-donating nature of the three hexyloxy moieties caused low shifts to negative potentials, and phenylacetylene spacer shift to positive potentials even if the shift was very slow.

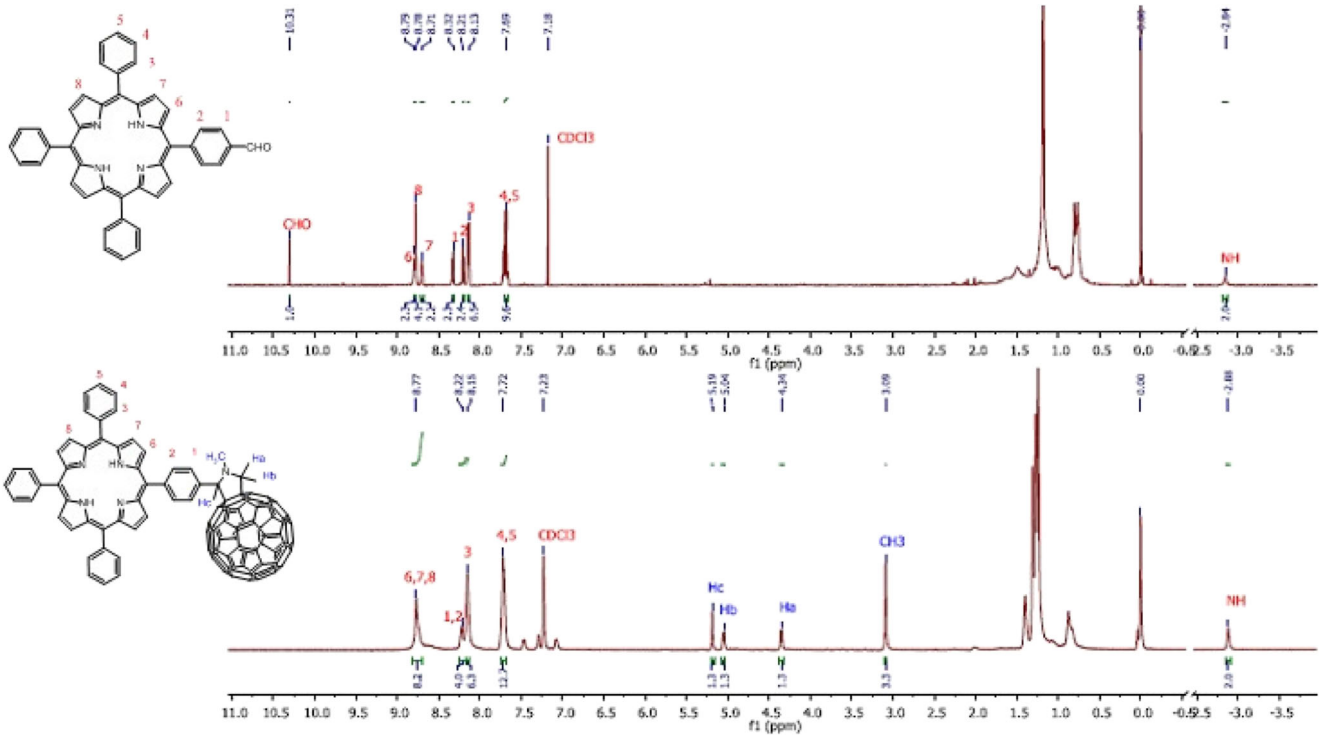

Fig. 2 ^{1}H NMR of **1-CHO** in $CDCl_3$ and dyad **1** in $CDCl_3/CS_2$ (1:1, v:v)

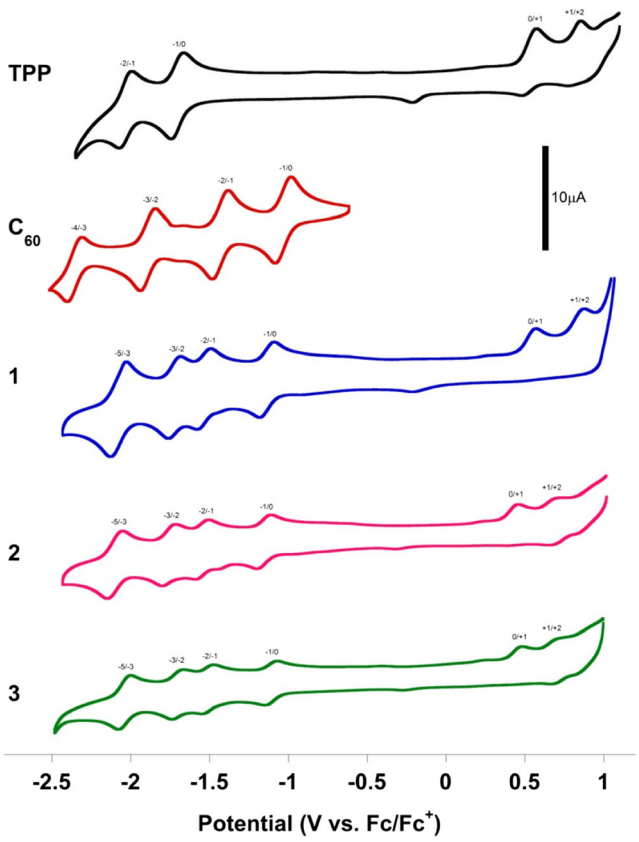

Fig. 3 Cyclic voltammetry profiles of **TPP**, fullerene C_{60} and dyads **1**–**3**, recorded in *o*-dichlorobenzene/acetonitrile (4:1) at 0.25 mM

HOMO and LUMO energy levels of the three dyads and of **TPP** were calculated using the first oxidation and first reduction values of the dyads in *o*-dichlorobenzene/acetonitrile (4:1) vs the HOMO level of ferrocen at −4.8 eV according to Eqs. 1 and 2 [39].

$$E_{HOMO} = -\left[\left(E_{ox} - E_{1/2(ferrocene)}\right) + 4.8\right] \quad (1)$$

$$E_{LUMO} = -\left[\left(E_{red} - E_{1/2(ferrocene)}\right) + 4.8\right] \quad (2)$$

As can be seen from Table 2, substituent and spacer affected the band gap very efficiently. In presence of fullerene moiety, band gaps remarkably decreased. The lowest band gap

Table 1 Redox potentials[a] of processes observed by cyclic voltammetry[b] (V vs Fc/Fc^+)

	E_{red4}	E_{red3}	E_{red2}	E_{red1}	E_{ox1}	E_{ox2}
TPP	-	-	-2.032	−1.704	0.530	0.815
C_{60}	-2.354	−1.890	−1.433	−1.033	-	-
1	−2.076	−1.723	−1.536	−1.134	0.572*	0.880*
2	−2.098	−1.758	−1.548	−1.156	0.416	0.690
3	−2.039	−1.701	−1.514	−1.108	0.481*	0.700

[a] All potential values as $E_{1/2} = (E_{pa} + E_{pc})/2$ and E_{pa} for * as exception. [b] Measured as 0.25 mManalyte in *o*-dichlorobenzene/acetonitrile (4:1), 0.1 M Bu_4NClO_4, scan rate 100 mV/s, $Ag/AgNO_3$ (0.01 M) reference electrode, Pt counter electrode, glassy carbon electrode, at room temperature

Table 2 Molecular orbital energy levels and HOMO–LUMO energy gaps determined from cyclic voltammetry (CV) and theoretical (th) calculations

Compound	$HOMO_{CV}$ (eV)	$LUMO_{CV}$ (eV)	$HOMO\text{-}LUMO_{CV}$ (eV)	$HOMO_{th}$ (eV)	$LUMO_{th}$ (eV)	$HOMO\text{-}LUMO_{th}$ (eV)
TPP	-5.330	−3.096	2.234	−5.159	−2.558	2.601
1	−5.372	−3.666	1.706	−5.217	−3.582	1.635
2	−5.216	−3.644	1.572	−4.997	−3.544	1.452
3	−5.281	−3.692	1.589	−5.006	−3.560	1.445

was found for molecule **2**, and this information matches the shortest absorption wavelength maxima of **2** compared to **1**, **3** and **TPP** (see Table 3).

Theoretical Calculations Structure optimization of the investigated dyads was performed first. Our calculated atomic structures of the dyads are depicted in Fig. 4 as ball-and-stick models. The structure optimizations were started from several initial configurations with reasonable bond lengths and continued until all force components are lower than 0.01 eV/Å in conjugate gradient algorithm. For our purposes, the overlap between the electronic states localized on the porphyrin and the π-conjugated bridge states of **3** is important since the π-conjugated bridge states are expected to be independent from the electronic states of the C_{60}. The electron transfer between the porphyrin core and the C_{60} moiety through the bridge is closely related to the dihedral angles between the phenyl rings of the bridge and the porphyrin core.

Although the phenyl rings were chosen in the plane of porphyrin cores, the phenyl rings are rotated during the structure optimizations. On each dyad, a porphyrin core is surrounded by 4 phenyl rings, and the dihedral angles between the porphyrin and phenyl planes were determined to be 66° in all structures. All calculations with a lower initial dihedral angle value ends up with this dihedral angle. We also find that the cost of rotating the phenyl rings to increase the dihedral angle is actually below the thermal energy of the room temperature. Therefore, at nonzero temperatures the dihedral angles may also be larger than the optimum value due to thermal vibrations. Because of this low energy threshold for phenyl ring rotations, the structure optimizations took at least thousand molecular dynamics steps. Our results indicate that the attachment of hexyloxy groups in **2** and **3** compared to **1** do not significantly affect the dihedral angles. The phenyl ring is connected to the C_{60} moiety through a sp^3 bonded C atom. The double bond on a hexagon-hexagon edge of the C_{60} is opened to convert the hybridization to sp^3 at the interface. In a sense the phenyl ring is the bridge between the porphyrin core and the C_{60}. The bridge contains an additional phenyl ring in dyad **3**, and the phenyl rings are joined by triple bonded C atoms. In the optimum structure, the two phenyl rings in the bridge are almost in the same plane. However, we observe that the rotation of the phenyl rings with respect to each other costs less than 20 meV and our structure optimizations go through very shallow energy landscape before reaching to this configuration. Therefore, at nonzero temperature the two phenyl rings may not be in the same plane due to thermal activation.

After obtaining fully relaxed atomic structures, electronic structures of the dyads **1–3** and **TPP** were calculated using GGA, HSE06, and B3LYP exchange-correlation functionals. As expected, GGA underestimates energy gaps, and this is corrected by hybrid Exchange-correlation functionals of B3LYP and HSE06. The HOMO and LUMO levels and energy gaps listed in Table 2 are calculated in B3LYP Exchange-correlation functional, which gives the best agreement with the experiment. Frontier orbitals of the three dyads are shown in Fig. 4 as 3D iso-density contour plots, where HOMO levels are indicated by blue-green colors and orange-turquoise colors are for LUMO levels. There are also several empty states above the LUMO that are localized on the C_{60} moiety, and several filled states below the HOMO level that are localized on the porphyrin core. The spatial localization of the frontier orbitals shown in Fig. 4 confirms that the porphyrin act as donor and the fullerene as acceptor, corroborating the cyclic voltammetry measurements.

The LUMO levels for all the dyads, shown in Fig. 4, are strictly localized on the C_{60} moiety because the sp^3 bonded carbon atoms help to confine the electronic states of the C_{60} with sp^2 character. The sp^3 bonding at the interface of the bridge and the fullerene isolates the electronic states of the

Table 3 Maximum absorption wavelengths (λ_{max}) and logarithmic values of molar extinction coefficients (ε) of dyads **1–3** and **TPP** in toluene

Compound	Soret or B(0–0)	Qy(1–0)	Qy(0–0)	Qx(1–0)	Qx(0–0)
TPP	419 (5.63)	514 (4.32)	548 (3.95)	591 (3.78)	648 (3.66)
1	420 (5.69)	515 (4.41)	549 (4.08)	591 (3.89)	648 (3.74)
2	424 (5.36)	518 (4.05)	555 (3.86)	595 (3.55)	651 (3.50)
3	424 (5.46)	518 (4.08)	555 (3.96)	595 (3.60)	652 (3.57)

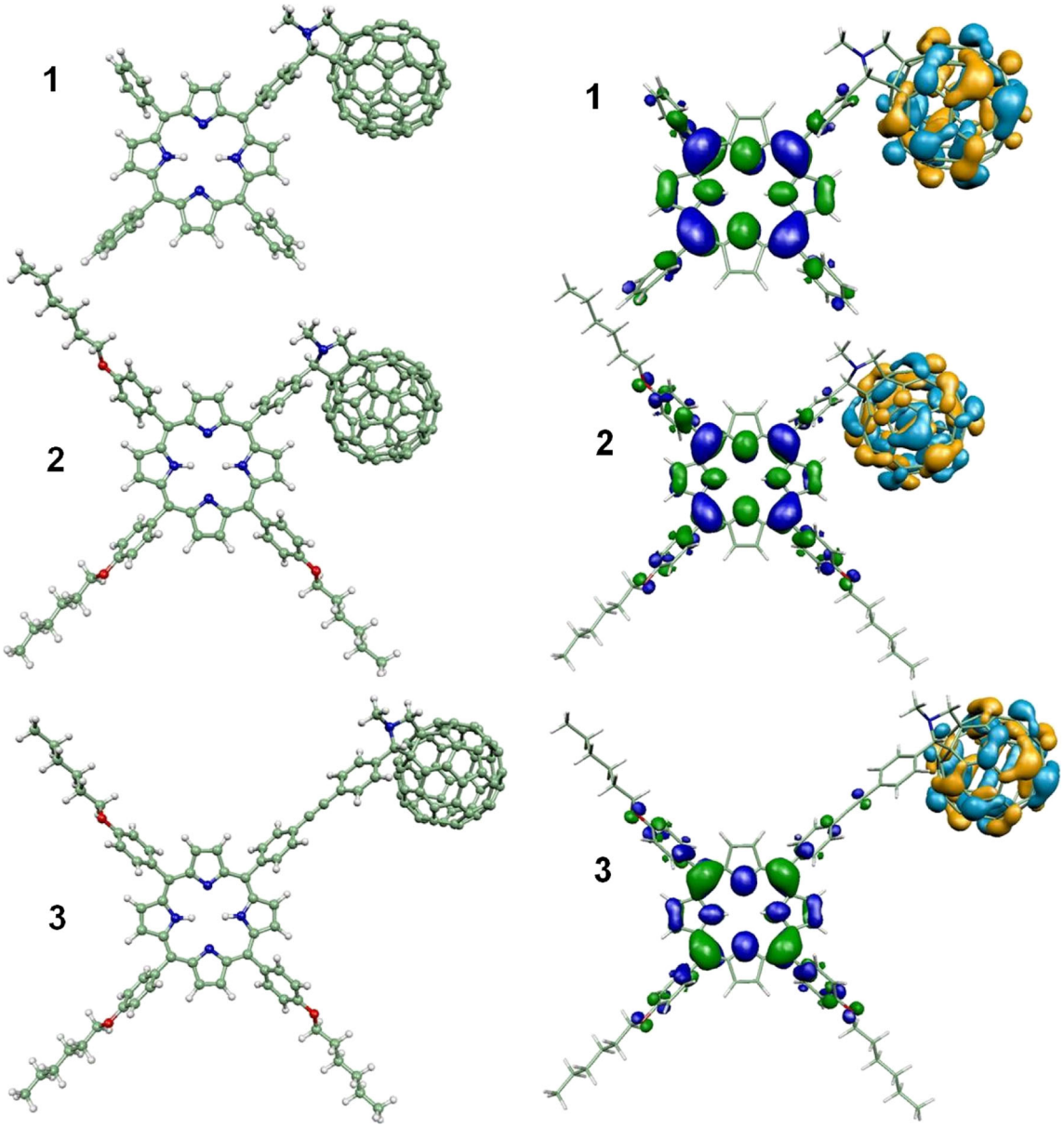

Fig. 4 Left: optimized geometries of dyads **1**, **2** and **3**. Right: HOMO-LUMO orbital schemes as resulted from DFT calculations displaying the donor and acceptor character of the dyads (the HOMOs and LUMOs are presented in navy blue-green and in orange-turquoise, respectively)

bridging phenyl rings, which are π-conjugated states near the HOMO and LUMO, from the fullerene states. Therefore, probability of charge transfer from the C_{60} moiety to the bridges is greatly reduced by this atomic configuration, playing an important role in delaying the deactivation of the electronic excited state through a radiative decay.

Unlike LUMO levels, HOMO levels of the dyads are localized on the porphyrin core and have π-state character. Since the phenyl rings are not in the plane of porphyrin core, the HOMO levels have very small contribution on the phenyl rings. The π-conjugated network is hindered by the rotation of the phenyl ring and thus the large dihedral angle of 66° is very crucial in isolating the HOMO level from the π-conjugated electronic states of the bridging phenyl rings. In fact, there would be no contribution from the phenyl ring to the HOMO if the dihedral angle was 90°, for which the phenyl ring is perpendicular to the porphyrin plane. In view of the fact that the dihedral angles larger than the optimum value is easily accessible by thermal activation as mentioned above, the HOMO level has very small overlap with the electronic states of the bridge. This also reduces the probability of radiative decay, giving time for the energy transfer to vibrational modes. Therefore, the large dihedral angle is a key structural parameter affecting the photophysical and photochemical properties.

In dyad **3**, the addition of a second phenyl ring to the bridge farther reduces the overlap between the HOMO level and the

π-conjugated bridge states since the HOMO does not penetrate to the second phenyl ring in dyad **3**, as shown in Fig. 4. Even a minute dihedral angle between the two phenyl rings of the bridge is enough to interrupt the π-conjugation network. Since even larger dihedral angles are possible under thermal excitations, the overlap between HOMO and the electronic states of the bridge is further reduced in dyad **3**. Therefore the inclusion of phenylacetylene in the bridge should suppress radiative decay, and allow better energy transfer to the vibration modes. On the basis of our calculations, we expect the highest photochemical activity for dyad **3.** In addition, it is expected that all dyads should have higher photochemical reactivity than **TPP** because of the reduced overlap between the HOMO and LUMO levels, and the isolation of the bridge states from these frontier orbitals, which is promoted by a large dihedral angle and the sp^3 bonded C atom.

Our calculated HOMO-LUMO energy gaps of 1.635, 1.452, and 1.445 eV for dyads **1**, **2**, and **3** respectively, are in good agreement with our experimentally measured values of 1.706, 1.572, and 1.589 eV. Our calculated HOMO and LUMO levels, listed in Table 2, indicate that the appearance of the acceptor level of the fullerene within the energy gap of **TPP** reduces the gap to 1.635 eV from 2.601 eV, the value for **TPP**. While introducing substituents do not affect the LUMO level located on the fullerene, the HOMO level is shifted up by the hexyloxy substituents, and thus reduces the energy gap, in agreement with our cyclic voltammetry results. This reduction of the energy gap decreases the lifetime of the excited state, and thus should decrease the photochemical activity since a faster electron transfer hinders the energy transfer to vibrations. However, in dyad **3,** the atomic structure plays a crucial role to prevent a radiative decay and thus should improve the photochemical activity. In case these structural factors dominate, the best photochemical activity should appear for dyad **3**. We expect better photochemical activity if the bridge contains longer phenylacetylene chain. Our molecular design provides non-overlapping donor and acceptor levels with a low electron transfer probability to allow a higher energy transfer to vibration modes. Our calculations indicate that the length of the bridge has very small effect on the energy levels and energy gaps, while the spacer is most likely to have an effect.

Choice of the Solvent for Photophysical and Photochemical Measurements

Our purpose is to investigate the interactions of the dyads at their excited states with molecular oxygen, which implies to promote energy transfer between the porphyrin and the fullerene units, and to limit or inhibit photo-induced electron transfer generating a charge separation, as these two events are competitive. The nature of the solvent chosen for photophysical and photochemical measurements is known to affect their outcome. Non-polar solvents such as toluene proved to be appropriate for such kind of measurements [40, 41]. The relevance of this choice had to be confirmed by checking the non-aggregation of the dyads **1**–**3** and the reference **TPP** to prevent aggregation-induced artefact results, as aggregation affects luminescence properties. Table 3 summarizes the UV-Vis bands and the extinction coefficients for porphyrin-fullerene dyads **1**–**3** as well as **TPP** as reference compound. The spectra exhibits a strong and sharp Soret band (at ~420–424 nm) and four weak Q-bands in the visible region between 515 and 652 nm due to a S0-S1 transition typical of free porphyrin. Beer-Lambert law plots (Fig. 5) are linear between 1 and 8 μM concentration range, and thus show no evidence for aggregation in this range.

The order of their maximum wavelengths was **3 = 2 > 1 > TPP** whereas the extinction coefficients show a quite different trends: **1 > TPP > 3 > 2** with respective log ε values of 5.69, 5.63, 5.46, 5.36. The small red shift between **TPP** and the fullerene-dyads **1**–**3** reveals a relatively shorter HOMO-LUMO gap. This effect is more pronounced when electron donating hexyloxy chains (of about 5 nm for **TPP** compared to **2** and **3**) are substituted on the porphyrin moieties. These observations are in accordance with the energy levels of the frontier molecule orbitals determined via electrochemical measurements.

Steady-State Fluorescence-Based Oxygen Sensitivity

As the fluorescence of free-base or metalloporphyrins is known to be strongly quenched by oxygen, either in solution or in solid matrices (thin films or nanofibers) [6, 7], they are interesting candidate for optical oxygen sensors. Steady-state fluorescence data, excitation and emission wavelengths, the Stokes shifts and the fluorescence quantum yields for dyads **1**–**3** and **TPP** were first determined and summarized in Table 4. The positions of the fluorescence emission maxima are very similar for dyads **1**–**3** and **TPP.** A noticeable quenching, 97%, 92% and 98% of pophyrin fluorescence by fullerene was observed for **1**, **2** and **3**, respectively. The fluorescence quantum yields Φ_F of the dyads **1**, **2** and **3** were found to be 0.003, 0.008 and 0.002, which can be considered as quasi-nul whereas the value for **TPP** (used as a reference standard) is 0.12 in DMF [42]. The presence of hexyloxy chains (comparison of **2** with **1**) increased Φ_F, but on the other hand dyad **3** exhibited the lowest Φ_F value in the series. This may be attributed to the spacer as generally triplet bonds shift the emission maxima to longer wavelength and decrease Φ_F.

The oxygen sensing properties of **TPP** and dyads **1**–**3** were investigated in toluene and the results are presented in Fig. 6. Despite the strong fluorescence quenching, dyads **1**, **2** and **3** shows still oxygen sensing ability. Especially the presence of three hexyloxy donating group on the porphyrin macrocycle influence the oxygen sensitivity, dyad **2** was the best oxygen sensing dyad in the series, even more sensitive than **TPP** (see

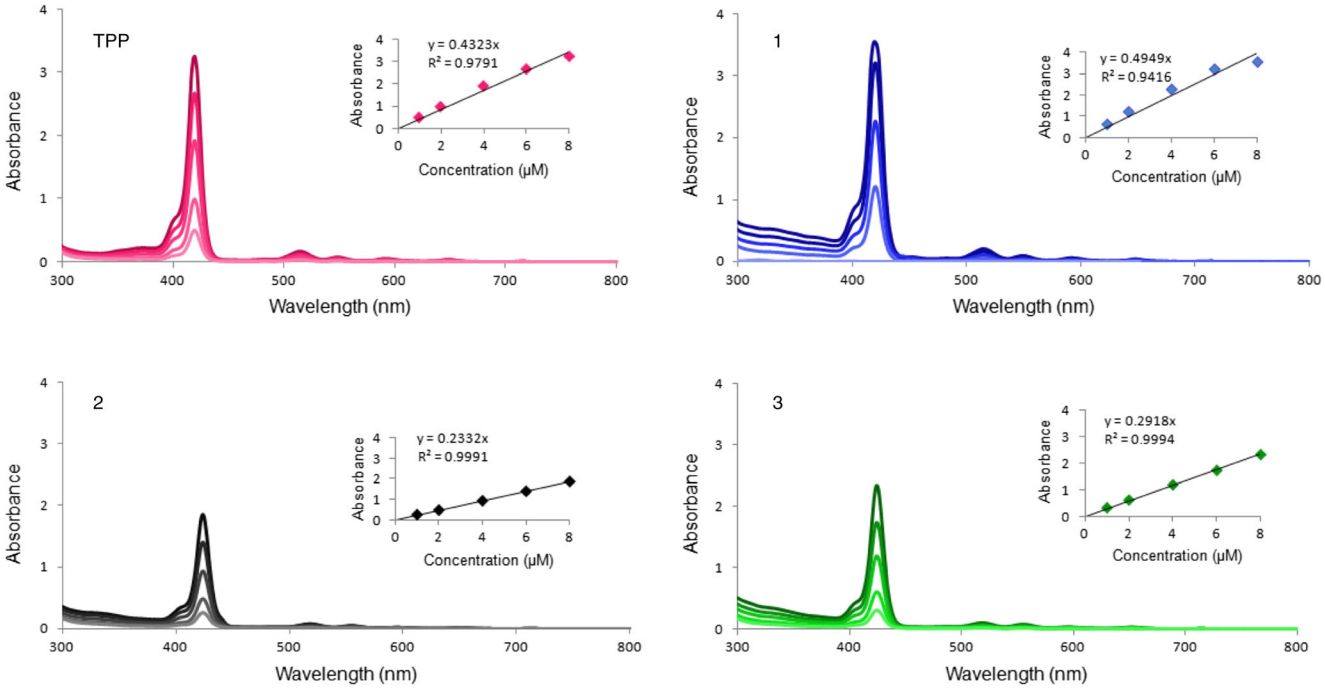

Fig. 5 Electronic absorptions of **TPP** and dyads **1**–**3** at 1, 2, 4, 6 and 8 μM. Inset: absorbance values vs concentration

Table 4), reaching an I_0/I_{100} value of 2.45. The presence of the phenylacetylene spacer in dyad **3** decreased the I_0/I_{100} ratio from 2.45 to 1.50, indicating a negative effect on the fluorescence-based oxygen sensitivity.

Singlet Oxygen Generation

Singlet oxygen generation is crucial in photodynamic processes, and a good photosensitiser must exhibit high singlet oxygen quantum yield (Φ_Δ). According to literature (from transition absorption/luminescence measurements), in non-polar solvent like toluene, the porphyrin-fullerene dyad behaviour is as follow: the singlet state of porphyrin is quenched by singlet-singlet energy transfer to the fullerene C_{60}, The singlet state of fullerene undergoes intersystem crossing to give the triplet state of fullerene, and this species have a high ability to react with triplet oxygen to form singlet oxygen.

The energy difference for the transition between the lowest energy of O_2 in the singlet state and the lowest energy in the triplet state is reported as 0.98 electron volts (eV), and it fits the energy gaps of porphyrins as well as the dyads **1–3** as calculated from cyclic voltammetry measurements [43]. In our study, Φ_Δ values of the dyads were determined by monitoring the phosphorescence of singlet oxygen at ~1270 nm in toluene. In more polar solvents, the stabilization of charge transfer state takes place, decreasing the efficiency of singlet oxygen generation [18]. Phosphorescence intensities of $^1O_2$ vs absorbance for **TPP** and the dyads **1**–**3** were presented in Fig. 7, and the quantum yields were summarized in Table 4. Φ_Δ values were calculated using **TPP** as a reference ($\Phi_\Delta = 0.63$ in toluene) [44], and appeared to be strongly affected by the presence of the fullerene, as all dyads have higher Φ_Δ values than **TPP**, with the following trend: **TPP** (0.63) < **2** (0.70) < **1** (0.78) < **3** (0.81). Dyad **3** exhibited the highest Φ_Δ respect to dyads **2** and **1**, in accordance with the lowest fluorescence quantum yield of **3** compared to **1** and **2**. It can be concluded that the presence of phenylacetylene linker between porphyrin and fullerene have a positive effect on singlet oxygen generation as the longer

Table 4 Photophysical and photochemical properties of **TPP** and dyads **1**–**3** in toluene (λ^{em}_{max}: maximum emission wavelength: Φ_F: fluorescence quantum yield and I_0/I_{100}: parameter exhibit oxygen sensitivity and singlet oxygen quantum yield)

Compound	λ^{em}_{max1} (nm)	λ^{em}_{max2} (nm)	Φ_F	Oxygen response (I_0/I_{100})	Φ_Δ
TPP	651	711	0.120[42]	1.79	0.63
1	653	715	0.003	1.35	0.78
2	653	715	0.008	2.45	0.70
3	653	715	0.002	1.50	0.81

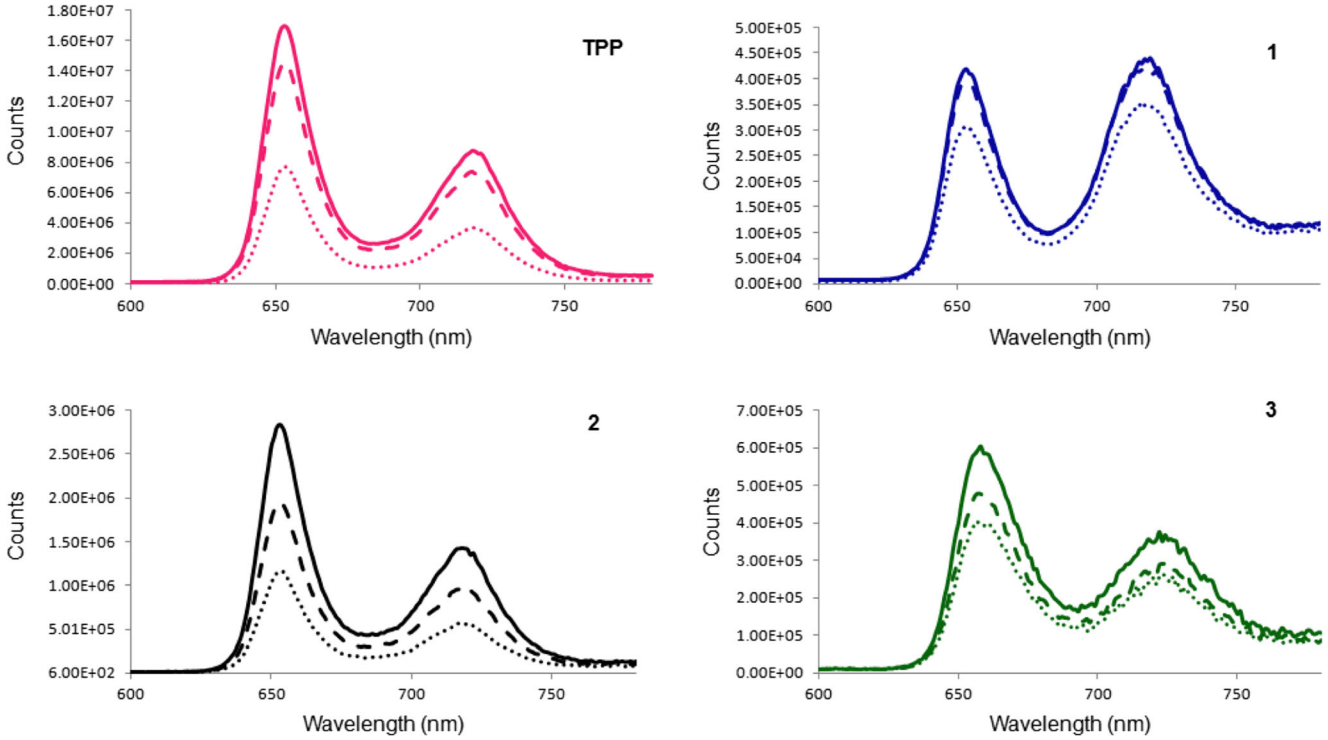

Fig. 6 Fluorescence spectra of **TPP** and the dyads **1**–**3** in toluene upon exposure to oxygen: 0% O_2 (–), 21% O_2 (–-), 100% O_2 (···)

distance between the donor and acceptor should favour the ISC transfer [23]. It should be also noted that for simple fullerene derivatives Φ_Δ is generally >0.9 [45]. These observations are somewhat opposed to those made for dyad with non-conjugated spacer [17] but in accordance with other reported trends [18].

Lifetime of singlet oxygen is an intrinsic characteristic like emission maxima of singlet oxygen (~1270 nm). It means that lifetime of singlet oxygen will not change depending on molecules but will depends on the medium. However, the count rate during the lifetime of singlet oxygen experiment will change from one molecule to another molecule in function of time.

Determination of singlet oxygen luminescence decay for **TPP** and dyads **1**–**3** in toluene have been recorded upon excitation by a spectra LED at 417 nm. Lifetime of singlet oxygen in toluene was found to be 31.4 ± 1.62 μs for all dyads and **TPP**, in accordance with the literature value; 29.4 ± 2.94 μs [46].

During 150 μs, the obtained counts were found to be 9500, 8700, 9800 and 7800 for dyads **1**, **2**, **3** and **TPP**, respectively. Dyad **3** exhibited the highest counts confirming that **3**

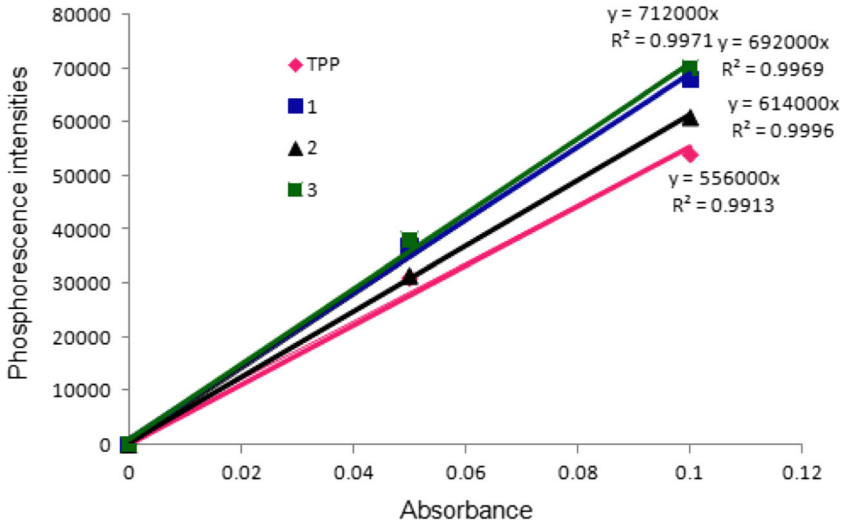

Fig. 7 Phosphorescence intensities of $^1O_2$ (at 1270 nm) vs absorbance for **TPP** and dyads **1**–**3**.λ^{ex}:405 nm

generates more $^1O_2$. These data confirm that our porphyrin-fullerene dyad, and in particular dyad **3**, is good candidates for biomedical applications, especially after making them water-soluble as recently reported for related derivatives [47].

Conclusions

A set of three porphyrin-fullerene dyads has been designed and prepared, thanks to a facilitated synthetic procedure of formylporphyrins, coupled afterwards to fullerene by the Prato reaction. Two structural parameters were varied: the presence of electron-donating hexyloxy chains at the *para* position of the *meso*-phenyl, and the presence of a phenylacetylene spacer between the porphyrin macrocycle and the fullerene. The effect of these structural variations on the electrochemistry, molecular orbital levels and energy gaps, ground state absorption, fluorescence and singlet oxygen generation of the dyads was comparatively investigated. These properties were interpreted with the final purpose to determine their suitability as oxygen sensors or photodynamic photosensitisers. Dyad **3** containing phenylacetylene spacer was found to be the best singlet oxygen generator as phenylacetylene increase the ISC process, whereas dyad **2** with hexyloxy chains but without spacer exhibited higher oxygen sensing ability. Probably because, when hexyloxy groups are introduced in the molecule, the HOMO-LUMO gap is affected noticeably. Dyad **2** could be a good candidate for further incorporation into doped microfilms/ nanofibers. Dyad **3** with hexyloxy chains and phenylacetylene spacer could be use in a next step in biomedical photodynamic applications making them water-soluble, retaining the alkyloxy chain pattern. Substituting the hexyloxy chains by polyethylene glycol chains could be a suitable option.

Experimental

Synthesis

Materials and Methods Starting materials were of reagent grade quality, purchased from Aldrich for Pyrrole (reagent grade 98%), n-Butyllithium 2.5 M solution in hexane and anhydrous *N,N*-dimethylformamide store over molecular sieve (Aldrich 40,248–250). Whereas diethylether dried max 0.005% H_2O (Merck 100,929) and propionic acid were purchased from Merck. Fullerene-C_{60}, *N*-Methylglycine (sarcosine), diisopropylamine, 4-ethynylbenzaldehyde were obtained from Aldrich. Preparative separations were performed by silica gel column chromatography Merck-60 (43–63 mesh) and TLC on aluminum sheets precoated with silica gel 60F254 (Merck). IR spectra were recorded between 4000 and 600 cm^{-1} using a Perkin Elmer Spectrum 100 FT-IR spectrometer with an attenuated total reflection (ATR) accessory featuring a zinc selenide (ZnSe) crystal. ^1H NMR spectra were recorded on a Varian 500 MHz spectrometer (with the deuterated solvents as the lock and tetramethylsilane as the internal reference). MALDI-MS spectra were acquired in linear modes with an average of 50 shots on a Bruker Daltonics Microflex mass spectrometer equipped with a nitrogen UV-Laser operating at 337 nm, using 2,5-dihydroxybenzoic acid or nitroanthracene as the matrix.

5-(4-Bromophenyl)-10,15,20-Triphenylporphyrin (1-Br) 4-bromobenzaldehyde (0.01 mol, 1.8 g), benzaldehyde (10.2 mL, 0.1 mol, 10 eqv.) were added to refluxing propionic acid (250 mL), then pyrrole (7.6 mL, 0.11 mol, 11 eqv.) was added to the reaction mixture. After refluxing for 1 h, the reaction mixture was cooled to room temperature and filtered. The filter cake was washed with methanol and hot water. The resulting crude mixture were purified on silica gel with *n*-hexane/DCM 2:1, 1/1 eluent system. **1-Br + TPP** could not be separated because of their close polarity. A clean mixture of **1-Br + TPP** (3 g) was obtained.

5-(4-Bromophenyl)-10,15,20-Tris(4-(Hexyloxyphenyl) Porphyrin (2-Br) 5-(4-bromophenyl)-10,15,20-tris(4-(hydroxy)phenylporphyrin (2.56 mmol, 1.9 g), hexyl bromide (51 mmol, 7.1 mL, 20 eqv.) and K_2CO_3 (20 g) were stirred in DMF (100 mL) at 60 °C over night and the reaction mixture was poured in water then washed with ethanol. Purification was achieved by column chromatography on silica gel with a gradient of eluent from DCM/hexane (1:1). Yield 43% (2.4 g). FT-IR: ν (cm^{-1}). 3315 (NH), 2950 (CH Ar), 1465 (C = N), 1399 (=C-N), 1174 (C-Hpyrrole), 966 porphyrin ring, 787 pyrrole ring, 726 (NH bending). ^1H NMR: δ (ppm), $CDCl_3$, −2.76 (s, 2H, NH), 1.02 (br, 9H, methyl-H), 1.27 (br,6H, CH_2(12), 1.49 (br,6H, CH_2(11), 1.67(m, 6H, CH_2(10), 2.04 (m, 6H,CH_2(9), 4.33 (t, 6H, CH_2(8), 7.53 (t, 2H, $_{CHAr\text{-}phenyl}$), 8.13 (br, 2H, $_{CHAr\text{-}phenyl}$), 8.49 (m, 12H, $CH_{Ar\text{-}phenyl}$), 8.81–8.89 (br, 8H, $CH_{pyrrole}$). MS-MALDI-TOF (*m/z*): $C_{62}H_{65}BrN_4O_3$ [calcd]: 994.131, [found]: 995.301 $[M + H]^+$. UV-vis: λ, nm, ($CHCl_3$) 418, 512, 547, 588, 644.

5-(4-Formylphenyl)-10,15,20-Triphenylporphyrin (1-CHO) A **TPP/1-Br** mixture (400 mg) was placed in a Schlenk tube and was dried by purge-and-refill for at least three times (nitrogen(g)/vacuum). Under nitrogen (g), dry diethylether (50 mL) was added with a syringe at room temperature. The purple solution was placed in a liquid nitrogen-acetone bath at −50 °C for 10 min. And a 5 mL of *n*-butyl lithium in hexane (2.5 M; 6.25 mmol) was added, giving rise to a green resulting mixture that was further stirred for 3 h at −50 °C. Then, dry DMF (5 mL, 37.5 mmol) was added. The cooling bath was removed and the green-blue reaction mixture

was stirred for 3 h more. At room temperature, HCl 5% (250 mL) was added and vigorously stirred for 15 min. The mixture was neutralized by NH_4OH. The resulting pink-red emulsion was extracted with chloroform, dried with Na_2SO_4 and evaporated to dryness at 45 °C. **1-CHO** free porphyrin (yield 35% 70 mg, calculated on the basis that 200 mg of **1-Br** were present in the TPP/1-Br mixture, as 200 mg of TPP were recovered) was purified by column chromatography eluted by diethyl ether/ DCM (1:9). Unreacted **TPP** (0.2 g) was recovered. FT-IR, ν (cm^{-1}): 3313 (NH), 3053 (CH_{Ar}), 1698 (C = O), 1601 (C = C_{phenyl}), 1568 (C = $C_{pyrrole}$), 1472 (C = N), 1154, ($CH_{pyrrole}$), 964($CH_{porp.\ Ring}$), 794 ($CH_{pyr.\ Ring}$), 720 (NH bending). ^{1}H NMR δ (ppm) $CDCl_3$: −2.84 (s, 2H, NH), 7.69 (m, 9H, CH(4,5), 8.13 (d, 6H, CH(3), 8.21 (d, 2H, CH(2), 8.32 (d, 2H, CH(1), 8.71 (d, 2H, $CH(7_{\text{-pyrrole}})$, 8.78 (s, 4H, $CH(8_{\text{-pyrrole}})$, 8.79 (d, 2H, $CH(6_{\text{-pyrrole}})$, 10.31 (s, H, CHO). MS-MALDI-TOF (*m/z*) $C_{45}H_{30}N_4O$ [calcd]: 642.762, [found]: 643.774 $[M + H]^+$. UV-vis (λ, nm) ($CHCl_3$) 420, 515, 559, 592, 649.

5-(4-Formylphenyl)-10,15–20-Tris(4-(Hexyloxyphenyl)Porphyrin (2-CHO) The same procedure as for **1-CHO** porphyrin was applied, starting from **2-Br** (0.2 g, 0.2 mmol), yielding 0.026 g (0.027 mmol, 13%) of **2-CHO**. FT-IR, ν (cm^{-1}): 3312 (NH), 2925 (CHAr), 1702(C = O), 1506 (C = Cphenyl), 1465 (C = N), 1173, (CHpyrrole), 966 (CH porph. Ring), 801 (CH pyr. Ring). ^{1}H NMR: δ (ppm), $CDCl_3$–2.72 (s, 2H, NH), 1.01 (b, 9H, methyl-H), 1.48,1.55 (b,12H, CH_2 (11,12), 1.66 (m, 6H, CH_2 (10), 2.01 (m, 6H,CH_2(9), 4.27 (t, 6H, CH_2(8), 7.31 (d, 6H, CH (3), 8.12 (d, 6H, CH(4), 8.31 (d, 2H, CH(2), 8.41(d, 2H,CH(1), 8.78 (d, 2H, $CH(5_{\text{-pyrrole}})$, 8.90 (s, 4H, CH ($7_{\text{-pyrrole}}$), 8.92 (d, 2H, $CH(6_{\text{-pyrrole}})$, 10.41 (s, 1H, CHO). MS-MALDI-TOF (*m/z*) $C_{63}H_{66}N_4O_4$ [calcd]: 942.508, [found]: 942.654 [M + H]. UV-vis (λ, nm) ($CHCl_3$) 424, 519, 555, 595, 652.

5-(4-Formylphenylethynyl)-10,15,20-Tris(4-(Hexyloxyphenyl)Porphyrin (3-CHO) In tri-necked reaction flask, **2-Br** (300 mg, 0.3 mmol), palladium(II) acetate (4 mg, 0.17 mmol) and triphenylphosphine (12 mg) were dissolved in degased mixture of dry diisiopropylamine and THF (35 mL/35 mL) under argon. 4-ethynylbenzaldehyde (0.117 g, 0.9 mmol, 3 eqv.) was added and the solution was refluxed for 2 days. Water (10 mL) was then added after cooling of the reaction mixture at room temperature. The resulting purple precipitate was filtered, and washed with hot water. Purification was achieved by column chromatography on silica gel with a gradient of eluent from DCM/hexane (1:2 then 1:1). Yield 24% (75 mg). FT-IR ν (cm^{-1}): 3316 (NH), 2950 (CHAr), 2216 (C ≡ C), 1699 (C = O), 1466 (C = N), 1174 (C–Hpyrrole), 966 (C–Hporp. ring), 790 (C–Hpyr. ring), 739 (NH bending). ^{1}H NMR: δ (ppm), $CDCl_3$, –2.70 (s, 2H, NH), 1.02(b, 9H, methyl-H), 1.49,1.55(b,12H, CH_2(10,11), 1.66(b, 6H, CH_2(9), 2.01 (b, 6H,CH_2(8), 4.27(b, 6H, CH_2(7), 7.30(b, 6H, $CH_2(5_{\text{-Ar-phenyl}})$, 7.83(b, 2H, $CH_2(2_{\text{Ar-phenyl}})$,7.96 (b, 4H, $CH(3,4_{\text{Ar-phenyl}})$, 8.14 (b, 6H,$CH(6_{\text{Ar-phenyl}})$, 8.27 (b, 2H, $CH(1_{\text{Ar-phenyl}})$, 8.86 (b, 2H, $CH_{pyrrole}$), 8.91 (s, 6H, $CH_{pyrrole}$), 10.08 (s, 1H, CHO). MS-MALDI-TOF (*m/z*) $C_{70}H_{71}N_4O_4$ [calcd]: 1043.365, [found]: 1043.227 [M + H]. UV-vis (λ, nm) ($CHCl_3$) 425, 519, 556, 595, 652.

General 1,3-Dipolar Cycloaddition Procedure for Dyads 1–3 A mixture of C_{60} (8 mg, 0.01 mmol), sarcosine (2 mg, 0.02 mmol, 2 eqv.), and 0.02 mmol (2 eqv) of **1-CHO** (12 mg), **2-CHO** (18 mg), **3-CHO** (20 mg) in toluene (60 mL) was refluxed for 2–5 h, then the solvent was removed under reduced pressure. The crude product was dissolved in toluene and purified over a silica gel column using toluene/ CS_2 (2:1 then 1:1) as the eluent.

Dyad 1 Yield 62%, 15 mg. FT-IR ν (cm^{-1}): 3314 (NH), 2920 (CHAr), 1463 (C = N), 1080 (C–Hpyrrole), 964 (C–Hporp. ring), 796 (C–Hpyr. ring), 72 (NHbending), 1185, 575, 525 (C_{60}). ^{1}H NMR δ (ppm), CS_2:$CDCl_3$ (1:1 v/v), −2.88 (s, 2H, NH), 3.09 (s, 3H, N-methyl-H), 4.34, 5.04, 5.19(d, d, s, pyrrolidine-H), 7.72 (b, 12H, $CH(4,5_{\text{Ar-phenyl}})$, 8.15 (b, 6H, $CH(3_{\text{Ar-phenyl}})$, 8.22 (b, 4H, $CH(1,2_{\text{Ar-phenyl}})$, 8.77 (b, 8H, $CH_{pyrrole}$). MS-MALDI-TOF (*m/z*) $C_{107}H_{35}N_5$ [calcd]: 1390.492, [found]: 1390.152 [M + H]. UV-vis (λ, nm) (toluene) 422, 516, 551, 593, 651.

Dyad 2 Yield 45%, 15 mg. FT-IR ν (cm^{-1}): 3311 (NH), 2919 (CHAr), 1465 (C = N), 1080 (C–Hpyrrole), 965 (C–Hporp. ring), 798 (C–Hpyr. ring), 732 ($NH_{bending}$), 574, 526 (C_{60}). ^{1}H NMR δ (ppm), CS_2:$CDCl_3$ (1:1, v:v), −2.80 (s, 2H, NH), 1.36, 1.39, 1.51 (b, 27H, CH_2(11,12, CH3), 1.68(b, CH_2(10), 2.01 (b,CH_2(9), 3.11 (s, 3H, N-methyl-H), 4.33, 5.05, 5.14 (d, d, s, pyrrolidine-H), 4.25(b, 6H, CH_2(8), 7.12 (d, 2H, $CH(2_{\text{Ar-phenyl}})$, 7.25 (d, 6H,$CH(3_{\text{Ar-phenyl}})$, 7.53 (d, 2H, $CH(1_{\text{Ar-phenyl}})$, 8.09 (d, 6H, $CH(4_{\text{Ar-phenyl}})$, 8.85 (s, 8H, $CH_{pyrrole}$). MS-MALDI-TOF (*m/z*) $C_{125}H_{71}N_5O_3$ [calcd]: 1690.975, [found]: 1690.632 [M + H]. UV-vis (λ, nm) (toluene) 424, 518, 555, 595, 651.

Dyad 3 Yield 55%, 10 mg. FT-IR ν (cm^{-1}): 3314 (NH), 2960 (CHAr), 1465 (C = N), 1086 (C–Hpyrrole), 1014 (C–Hporp. ring), 794 (C–Hpyr. ring), 721 (NHbending), 525 (C_{60}). ^{1}H NMR δ (ppm), CS_2:$CDCl_3$ (1:1 v/v), −2.86 (s, 2H, NH), 0.94 (b, 9H, methyl-H), 1.41 (b,12H, CH_2(10,11), 1.58 (b, 6H, CH_2(9), 1.93 (b, 6H, CH_2(8), 2.78 (s, 3H, N-methyl-H), 3.74, 4.85, 5.23 (d, d, s, pyrrolidine-H), 4.18(b, 6H, CH_2(7), 7.19 (b, 6H, $CH(5_{\text{Ar-phenyl}})$, 7.66 (b, 2H, $CH(2_{\text{Ar-phenyl}})$, 7.82 (b, 4H, $CH(3,4_{\text{Ar-phenyl}})$, 8.01(b, 6H,$CH(6_{\text{Ar-phenyl}})$, 8.11 (b, 2H, $CH(1_{\text{Ar-phenyl}})$, 8.78 (b, 8H, $CH_{pyrrole}$). MS-MALDI-TOF (*m/z*) $C_{133}H_{75}N_5O_3$ [calcd]: 1791.095, [found]:

1790.634 $[M + H]^-$. UV-vis (λ, nm) (toluene) 424, 518, 555, 595, 652.

Photophysical and Photochemical Measurements

Absorption Optical spectra in the UV-visible region were recorded on a Shimadzu 2001 UV spectrophotometer using a 1 cm path length cuvette.

Steady-State Luminescence Emission Steady-state luminescence emission spectra were recorded using a Horiba–JobinYvon Fluorolog-3spectrofluorimeter (FL3-2IHR).

Fluorescence Quantum Yield Determinations In our study, *meso*-tetraphenylporphyrin **(TPP)** ($\Phi_F = 0.12$ in toluene [42]) was used as reference standard. Absorbance and luminescence spectra of the dyadsand of the reference **TPP** were measured under identical conditions (absorbance at both the excitation wavelengths were 0.05). All solutions were thoroughly deoxygenated by nitrogen bubbling through for 3 min. The ratio of the integrated luminescence intensities of the sample to reference standard was compared to find out quantum yield thanks to following Equation.

$$(\varphi_F)_X = (\varphi_F)_{ST}\left(\frac{Grad_X}{Grad_{ST}}\right)$$

Singlet Oxygen Quantum Yield Determination Singlet oxygen productions were measured in toluene by optical method which are based on comparison between singlet molecular oxygen phosphorescence in the near infrared region at ~1270 nm produced by the corresponding dyads and the reference photosensitiser, **TPP** ($\Phi_\Delta = 0.63$ in toluene) [44]. Phosphorescence signal of $^1O_2$ was recorded by Horiba-JobinYvon Fluorolog-3R spectrofluorimeter using 450 W Xe arc lamp as a light source equipped with high sensitive Hamamatsu PMT cooled housing detector (300–1700 nm). In this system, a high cut filter (1250 nm) was used in order to prevent the interference light below 1250 nm. For this purpose, the absorbance and phosphorescence measurements of **TPP** and all dyads were carried out at two different concentrations. The phosphorescence intensities were plotted vs absorbance for **TPP** and corresponding dyads. Singlet oxygen quantum yields (Φ_Δ) were calculated according to following Equation using the ratio of the gradients.

$$(\varphi_\Delta)_X = (\varphi_\Delta)_{ST}\left(\frac{Grad_X}{Grad_{ST}}\right)$$

Singlet Oxygen Lifetime Measurements Phosphorescence lifetime of $^1O_2$ was recorded by Horiba–JobinYvon Fluorolog-3R spectrofluorimeter using a pulsed diode (SpectraLED −415 emitting 417 nm) as a light source equipped with high sensitive Hamamatsu PMT cooled housing detector (300–1700 nm) in presence of high cut filter (1250 nm). The system is monitored by a (TCSPC) system with the software DataStation and DAS6 (Horiba JobinYvon).

Oxygen Sensing Measurements Oxygen and nitrogen gases were mixed in the concentration range 0–100% in a gas diluter (Sonimix 7000A gas blending system). The total pressure was maintained at 760 Torr. The output flow rate of the gas mixture was maintained at 550 mL min^{-1}. Gas mixtures were introduced into the sensing agent containing cuvette via a diffuser needle under ambient conditions.

Electrochemical Measurements

Supporting electrolyte, n-Bu_4NClO_4 was purchased from Aldrich and dried overnight at 50 °C under vacuum. Ferrocene was supplied by Fluka, anhydrous acetonitrile by VWR and 1,2-dichlorobenzene by Merck. 3 mm-diameter glassy carbon working electrode (CHI104), non-aqueous Ag/Ag + reference electrode with porous teflon tip (CHI112), platinum wire counter electrode (CHI115) and electrode polishing kit (CHI120) were purchased from CH Instruments. Measurements were carried out on CH Instruments 842B model work station. The setup was conventional three-electrode cell equipped with glassy carbon working electrode, platinum wire counter electrode, and Ag/$AgNO_3$ reference electrode. The glassy carbon electrode was polished routinely with 0.05 μm alumina powder/water slurry on pads before running experiments. All measurements of samples were recorded as reported analyte concentration in 0.1 M n-Bu_4NClO_4 electrolyte solutions of o-dichlorobenzene/acetonitrile (4:1) mixture. Analyte solutions were deaerated with Argon purge for 5 min and kept under blanket of argon during the experiments. All electrochemical measurements were performed at ambient temperature. Ferrocene was used as internal reference and all potentials were referenced to ferrocene/ferrocenium (Fc/Fc+) redox couple. Potentials were reported versus ferrocene/ferrocenium (Fc/Fc+) redox couple. Scan rate was 100 mV/s for all CV experiments.

Computational

Structure optimization and electronic structure calculations are performed in density functional theory. Because of the soft vibration modes the structure optimizations are found to be very demanding, and reuire at least thousand molecular dynamic steps. We use revised Perdew-Burke-Ernzerhof (revPBE) [48]. Generalized Gradient Approximation (GGA) functional for exchange-correlationas implemented in the SIESTA [49] code. Electronic wavefunctions are expanded to a double-ζ basis set augmented by polarization orbitals.

The interaction between the core and valence electrons are handled by Troullier-Martins norm-conserving pseudopotentials [50] in their fully separable form [51]. Geometry optimizations in the conjugate-gradient algorithm are continued until all force components on each atom is less than 0.01 eV/Å. Since GGA underestimates fundamental energy gaps, electronic energy levels are calculated also in HSE06 and B3LYP hybrid exchange-correlation functionals using 6-311G** basis set as implemented in NWChem computer code [52]. Both computer codes give the same energy levels for GGA functional. The value of HOMO-LUMO energy gaps are in the best agreement with the experiment for B3LYP exchange-correlation functional.

Acknowledgements Catherine Hirel, Emel Önal and Sevinc Z. Topal acknowledge the Scientific and Technical Research Council of Turkey (TUBITAK) for their financial support through the project 111 M139. The authors thank also Eren Jason Gürbüz for the graphical design of Fig. 1.

References

1. Zhao J, Wu W, Sun J, Guo S (2013) Triplet photosensitizers: from molecular design to applications. Chem Soc Rev 42:5323–5351
2. Ghogare AA, Greer A (2016) Using singlet oxygen to synthesize natural products. Chem Rev 116:9994–10034
3. Topkaya D, Ng S.Y, Bretonnière Y, Lafont D, Chung L Y, Lee H B, Dumoulin F (2016) Iodination improves the phototoxicity of an amphiphilic porphyrin. Photodiagn Photodyn Ther, 16: 12–14
4. Topkaya D, Lafont D, Poyer F, Garcia F, Albrieux F, Maillard P, Bretonnière Y, Dumoulin F (2016) Design of an amphiphilic porphyrin exhibiting high in vitro photocytotoxicity. New J Chem 40: 2044–2050
5. Topkaya D, Arnoux P, Dumoulin F (2015) Modulation of singlet oxygen generation and amphiphilic properties of trihydroxylated monohalogenated porphyrins. J Porphyrins Phthalocyanines 19: 1081–1087
6. Topal SZ, Önal E, Ertekin K, Oter O, Gürek AG, Hirel C (2013) Significant sensitivity and stability enhancement of tetraphenylporphyrin-based optical oxygen sensing material in presence of perfluorochemicals. J. Porphyrins Phthalocyanines 17:431–439
7. Önal E, Ay Z, Yel Z, Ertekin K, Gürek AG, Topal SZ, Hirel C (2016) Design of oxygen sensing nanomaterial: synthesis, encapsulation of phenylacetylide substituted Pd(II) and Pt(II) meso-tetraphenylporphyrins into poly(1-trimethylsilyl-1-propyne) nanofibers and influence of silver nanoparticles. RSC Adv 6:9967–9986
8. Guldi DM (2002) Fullerene-porphyrin architectures; photosynthetic antenna and reaction center models. Chem Soc Rev 31:22–36
9. Conoci S, Guldi MD, Nardis S, Paolesse R, Kordatos K, Prato M, Ricciardi G, Vicente MGH (2004) Zilbermann I, Valli L. Langmuir–Shäfer transfer of fullerenes and porphyrins: formation, deposition, and application of versatile films. Chem Eur J 10:6523–6530
10. Yamada K, Imahori H, Nishimura Y, Yamazaki I, Sakata Y (1999) Acceleration of Photoinduced charge separation in porphyrin-C_{60} dyad with an acetylene spacer. Chem Lett 28:895–896
11. Imahori H, Sakata Y (1999) nFullerenes as novel acceptors in photosynthetic electron transfer. Eur. J. Org. Chem. 10,:2445-2457
12. Gust D, Moore TA, Moore AL (2001) Mimicking photosynthetic solar energy transduction. Acc Chem Rev 34:40–48
13. Imahori H, El-Khouly ME, Fujitsuka M, Ito O, Sakata Y, Fukuzumi S (2001) Solvent dependence of charge separation and charge recombination rates in porphyrin−fullerene dyad. J Phys Chem A 105:325–332
14. Kodis G, Liddell PA, Garza L, Clausen PC, Lindsey JS, Moore AL, Moore TA, Gust D (2002) Efficient energy transfer and electron transfer in an artificial photosynthetic antenna−reaction center complex. J Phys Chem A 106:2036–2048
15. Imahori H, Yamada H, Guldi DM, Endo Y, Shimomura A, Kundu S, Yamada K, Okada T, Sakata Y, Fukuzumi S (2002) Comparison of reorganization energies for intra- and intermolecular electron transfer. Angew Chem Int Ed 41:2344–2347
16. Tkachenko NV, Lemmetyinen H, Sonoda J, Ohkubo K, Sato T, Imahori H, Fukuzumi S (2003) Ultrafast Photodynamics of Exciplex formation and Photoinduced electron transfer in porphyrin−fullerene dyads linked at close proximity. J Phys Chem A 107: 8834–8844
17. Schuster DI, MacMahon S, Guldi DM, Echegoyen L, Braslavsky SE (2006) Synthesis and photophysics of porphyrin–fullerene donor–acceptor dyads with conformationally flexible linkers. Tetrahedron 62:1928–1936
18. Milanesio ME, Alvarez MG, Rivarola V, Silber JJ, Durantini EN (2005) Porphyrin-fullerene C_{60} dyads with high ability to form photoinduced charge-separated state as novel sensitizers for photodynamic therapy. Photochem Photobiol 81:891–897
19. Ballatore MB, Spesia MB, Milanesio ME, Durantini EN (2014) Synthesis, spectroscopic properties and photodynamic activity of porphyrin–fullerene C_{60} dyads with application in the photodynamic inactivation of *Staphylococcus aureus*. Eur J Med Chem 18:685–694
20. Constantin C, Neagu M, Ion RM, Gherghiceanu M, Stavaru C (2010) Fullerene–porphyrin nanostructures in photodynamic therapy. Nanomedicine 5:307–317
21. Huang L, Terakawa M, Zhiyentayev T, Huang Y-Y, Sawayama Y, Jahnke A, Tegos GP, Wharton T, Hamblin MR (2010) Innovative cationic fullerenes as broad-spectrum light-activated antimicrobials. Nanomedicine: NBM 6:442–452
22. Wu H, Fan S, Jin X, Zhang H, Chen H, Dai Z, Zou X (2014) Construction of a zinc porphyrin–fullerene-derivative based Nonenzymatic electrochemical sensor for sensitive sensing of hydrogen peroxide and nitrite. Anal Chem 86:6285–6290
23. Obondi CO, Lim GN, Churchill B, Poddutoori PK, Est A, D'Souza F (2016) Modulating the generation of long-lived charge separated states exclusively from the triplet excited states in palladium porphyrin–fullerene conjugates. Nano 8:8333–8344
24. Prato M, Maggini M (1998) Fulleropyrrolidines: a family of full-fledged fullerene derivatives. Acc Chem Res 31:519–526
25. Tagmatarchis N, Prato M (2003) The addition of azomethine ylides to [C_{60}]fullerene leading to fulleropyrrolidines. Synlett 3:768–779
26. Maggini M, Scorrano G, Prato M (1993) Addition of azomethine ylides to C_{60}: synthesis, characterization, and functionalization of fullerene pyrrolidines. J Am Chem Soc 115:9798
27. Nierengarten JF, Eckert F, Nicoud JF, Ouali L, Krasnikov V, Hadzioannou G (1999) Synthesis of a C_{60}-oligophenylenevinylene hybrid and its incorporation in a photovoltaic device. Chem Commun 617–618. doi:10.1039/A900829B
28. Ding H, Meng X, Cui X, Yang Y, Zhou T, Wang C, Zeller M, Wang C (2014) Highly-efficient synthesis of covalent porphyrinic cages via DABCO-templated imine condensation reactions. Chem Commun 50:11162–11164
29. Önal E, Ahsen V, Pécaut P, Luneau D, Hirel C (2015) Bromine–lithium exchange as a straightforward method to obtain meso-tetrakis(4-formylphenyl)porphyrin: a versatile intermediate. Tetrahedron Lett 56:5157–5160
30. Lembo A, Tagliatesta P, Guldi DM, Wielopolski M, Nuccetelli M (2009) Porphyrin−β-oligo-ethynylenephenylene−[C_{60}]fullerene

triads: synthesis and electrochemical and photophysical characterization of the new porphyrin−oligo-PPE−C_{60}fullerene systems. J Phys Chem A 113:1779–1793

31. Adler AD, Longo FR, Finarelli JD, Goldmacher J, Assour J, Korsakoff LA (1967) Simplified synthesis for meso-tetraphenylporphine. J Org Chem 32:476
32. Hirsch A, Brettreich M (2005) In fullerenes. Wiley-VCH Verlag GmbH & Co. KGaA, ch1, pp 1–48. doi:10.1002/3527603492
33. Schettino V, Pagliai M, Ciabini L, Cardini G (2001) The vibrational spectrum of fullerene C_{60}. J Phys Chem A 105:11192–11196
34. Drovetskaya T, Reed CA, Boyd P (1995) A fullerene porphyrin conjugate. Tetrahedron Lett 36(44):7971–7974
35. Ishida M, Park SW, Hwang D, Koo YB, Sessler JL, Kim DY, Kim D (2011) Donor-substituted β-functionalized porphyrin dyes on hierarchically structured mesoporous TiO_2 spheres. Highly efficient dye-sensitized solar cells. J Phys Chem C 115:19343–19354
36. Maggini M, Karlsson A, Scorrano G, Sandonà G, Farnia G, Prato M (1994) Ferrocenyl fulleropyrrolidines: a cyclic voltammetry study. J Chem Soc Chem Commun 5:589–590. doi:10.1039/C39940000589
37. Tu Y-J, Cheng H C, Chao I, Cho C-R, Cheng R-J, Su YO (2012) Intriguing electrochemical behavior of free base porphyrins: effect of porphyrin–*meso*-phenyl interaction controlled by position of substituents on *meso*-phenyls. J Phys Chem A 116:1632–1637
38. Pelado B, Abou-Chahine F, Calbo J, Caballero R, de la Cruz P, Junquera-Hernandez JM, Orti E, Tkachenko NV, Langa F (2015) Role of the bridge in photoinduced electron transfer in porphyrin–fullerene dyads. Chem Eur J 21:5814–5825
39. Thelakkat M, Schmidt HW (1998) Synthesis and properties of novel derivatives of 1,3,5-tris(diarylamino)benzenes for electroluminescent devices. Adv Mater 10:219–223
40. Kuciauskas D, Lin S, Seely GR, Moore AL, Moore TA, Drovetskaya T, Reed C A, Boyd PDW (1996) Energy and photo-induced electron transfer in porphyrin−fullerene dyads. J Phys Chem 100:15926–15932
41. Schuster DI (2000) Synthesis and photophysics of new types of fullerene–porphyrin dyads. Carbon 38:1607–1614
42. Owens JW, Smith R, Robinson R, Robins M (1998) Photophysical properties of porphyrins, phthalocyanines, and benzochlorins. Inorg Chim Acta 279(2):226–231
43. Shinohara H, Tsaryova O, Schnurpfeil G, Wöhrle D (2006) Differently substituted phthalocyanines: comparison of calculated energy levels, singlet oxygen quantum yields, photo-oxidative stabilities, photocatalytic and catalytic activities. J Photochem Photobiol A Chem 184(1–2):50–57
44. Redmond RW, Gamlin JN (1999) A compilation of singlet oxygen yields from biologically relevant molecules. Photochem Photobiol 70(4):391–475
45. Arbogast JW, Darmanyan AP, Foote CS, Rubin Y, Diederich FN, Alvarez MM, Anz SJ, Whetten RL (1991) Photophysical properties of sixty atom carbon molecule (C_{60}). J Phys Chem 95:11–12
46. Salokhiddinov KI, Byteva IM, Gurinovich GP (1981) Lifetime of singlet oxygen in various solvents. J Appl Spectrosc 34(5):561–564
47. Guan M, Qin T, Ge J, Zhen M, Xu W, Chen D, Li S, Wang C, Su H, Shu C (2015) Amphiphilic trismethylpyridylporphyrin-fullerene (C_{70}) dyad: an efficient photosensitizer under hypoxia conditions. J Mater Chem B 3(5):776–783
48. Perdew JP, Burke K, Ernzerhof M (1996) Generalized gradient approximation made simple. Phys Rev Lett 77(18):3865–3868
49. Soler JM, Artacho E, Gale JD, García A, Junqueran J, Ordejón P, Sánchez-Portal D (2002) The Siesta method for ab initio order-N materials simulation. J Phys: Condens Matt 14:2745–2779
50. Troullier N, Martins JL (1991) Efficient pseudopotentials for plane-wave calculations. Phys Rev B 43:1993–2006
51. Kleinman L, Bylander DM (1982) Efficacious form for model pseudopotentials. Phys Rev Lett 48(20):1425–1428
52. Valiev M, Bylaska EJ, Govind N, Kowalski K, Straatsma TP, Van Dam HJJ, Wang D, Nieplocha J, Apra E, Windus TL, de Jong WA (2010) NWChem: a comprehensive and scalable open-source solution for large scale molecular simulations. Comput Phys Commun 181(9):1477–1489